Electron concentration effects on the Shastry-Sutherland phase stability in $Ce_{2-x}Pd_{2+y}In_{1-z}$ solid solutions

J. G. Sereni,[1] M. Giovannini,[2] M. Gómez Berisso,[1] and A. Saccone[3]
[1]*Div. Bajas Temperaturas, Centro Atómico Bariloche (CNEA) and Conicet, 8400 S.C. Bariloche, Argentina*
[2]*CNR-SPIN and Dipartimento di Chimica e Chimica Industriale, Università di Genova, I-16146 Genova, Italy*
[3]*Dipartimento di Chimica e Chimica Industriale, Università di Genova, I-16146 Genova, Italy*
(Received 18 October 2010; published 23 February 2011)

The stability of the Shastry-Sutherland (ShaSu) phase as a function of electron concentration is investigated through the field dependence of thermal and magnetic properties of the solid solution $Ce_{2-x}Pd_{2+y}In_{1-z}$ on the antiferromagnetic (AF) branch. In these alloys, the electronic (holes) variation is realized by increasing Pd concentration. The AF transition T_M decreases from 3.7 to 3.0 K as Pd concentration increases from $y = 0.2$ to 0.4. By applying magnetic field, the ShaSu phase is suppressed once the field-induced ferromagnetic polarization takes over at a critical field B_{cr}, which increases with Pd content. A detailed analysis around the critical point reveals a structure in the maximum of the $\partial M/\partial B$ derivative, which is related to an incipient step in the magnetization $M(B)$ predicted by the theory for the ShaSu lattice. The crossing of $M(B)$ isotherms, observed in ShaSu prototype compounds, is also analyzed. The effect of In substitution by Pd is interpreted as an increase in the number of "holes" of the conduction band and results in a unique parameter able to describe the variation of the magnetic properties along the studied range of concentration.

DOI: 10.1103/PhysRevB.83.064419 PACS number(s): 75.30.−m, 75.40.Cx, 75.10.Jm

I. INTRODUCTION

Magnetic frustration is an attractive topic in physics since it may drive the systems to new and exotic phases.[1] Frustration originates mostly in peculiar geometrical conditions that impede the development of long-range order. One of the simplest examples of magnetic frustration is the triangular coordination of moments interacting antiferromagnetically among them. Since a canonical antiferromagnetic (AF) minimum of energy cannot be reached, the system accesses alternative minima where other types of order parameters may develop.

In the presence of AF interactions, Shastry-Sutherland (ShaSu) lattices[2] present those characteristics because neighboring magnetic atoms are disposed in triangular arrangements. In the model compound $SrCu_2(BO_3)_2$,[3] magnetic Cu^{2+} atoms have one nearest-neighbor (NN) and four next-nearest neighbors (NNN) on the same plane, all of them coupled antiferromagnetically by respective J and J' exchanges. Since the effective interactions are $J > J'$, NN atoms form a network of J mediated orthogonal dimers, being the interaction between dimers mediated by J'. As a result, the magnetic structure can be described as a quasi-two-dimensional lattice of orthogonal dimers.[4]

Two significant features were observed in the field B-dependent magnetization M curves of $SrCu_2(BO_3)_2$:[3] (i) a crossing of the magnetization isotherms at low temperature ($T < 4$ K) and (ii) two small steps in $M(B)$ at fractional values (cf. 1/4 and 1/8) of the saturation moment M_{sat}. In this compound, those steps are observed at a quite high applied magnetic field $B \approx 20$ T.[3] This so-called "quantized magnetization" scenario, with $M = 1/2, 1/4, 1/8, \ldots$ of M_{sat} is explained by the theory [4] as due to successive commensurate shells of two-dimensional (2D) squares involving an integer number of dimers. This model considers the geometrical distribution of the magnetic entities (i.e., dimers) as topologically equivalent to the 2D square lattice of the Heisenberg model. A simple series expansion according to $N = 2^n$, where n is an integer number $n = 1,2,\ldots$, accounts for the number of dimers N involved in the successive shells as the magnetic field increases. As a consequence of the J-AF character, the fourfold state of the dimers splits into a ground singlet and an excited triplet.[4]

Among intermetallic compounds, some heavy rare-earth tetraborides RB_4 (Ref. 5) were found to show these features but at lower magnetic field, for example, 4 T for ErB_4, with a clear step at $1/2M_{sat}$. A similar scenario was invoked in Yb_2Pt_2Pb,[6] which shows AF order at $T_M \approx 2$ K. Within the Mo_2B_2Fe-type structure, there is a large family of compounds with the formula R_2T_2X, where T is a transition metal and X is a p metal. In this structure, the magnetic atoms R are disposed in a unique crystalline site. Particularly, those compounds with T = Pd and X = Sn (Ref. 7) or In (Ref. 8) are of interest concerning the ShaSu phase formation because of the triangular coordination of the R magnetic atoms. This quasi-2D structure can be described as successive $T + X$ (at $z = 0$) and R (at $z = 1/2$) layers,[9] with the R NN and NNN disposed with the same symmetry as in $SrCu_2(BO_3)_2$, albeit at different relative distances.

A ShaSu phase was also reported in Ce_2Pd_2Sn (Ref. 10) within a limited range of temperature, that is, between an AF transition at $T_M = 4.9$ K and a ferromagnetic (FM) one of first-order type at $T_C = 2.1$ K. Since in this compound the dimer's formation is mediated by a J-FM exchange, the previously mentioned triplet has the lowest energy. The ShaSu phase is built by a J'-AF exchange below $T_M = 4.9$ K, however it becomes unstable below $T_C = 2.1$ K when the interplane FM interaction J_C takes over, inducing a 3D-FM ground state (GS).

The ShaSu phase is suppressed under a relatively low magnetic field at a magnetic critical point: $B_{cr} = 0.11$ T and $T_{cr} = 4.1$ K.[11] Despite the low B_{cr} value, isothermal $M(B)$ measurements show the features observed in the mentioned ShaSu model compounds, that is, the crossing of

magnetization isotherms and an incipient step as a function of field at $M \approx 1/4 M_{sat}$.

The stability of the ShaSu phase was also investigated under structural pressure, by doping Pd with smaller isoelectronic Ni atoms. The expected weakening of the Ce magnetic moment and the increase of the Sommerfeld coefficient γ occurs in $Ce_2(Pd_{1-x}Ni_x)_2Sn$ as the Kondo screening increases. The upper transition temperature T_M decreases with Ni content due to the weakening of the J exchange.[12] On the contrary, the lower transition T_C to the FM phase increases with x(Ni) as a consequence of the reduction of the temperature range of the ShaSu stability because of the weakening of the J' coupling. Both J and J' are overcome by the inter-Ce planes coupling in the "c" crystalline direction J_C, which for $x = 0.25$ practically inhibits the ShaSu phase formation.

Besides magnetic field and structural pressure, the third complementary control parameter to be used to investigate this ShaSu phase stability is the chemical potential variation. In this family of compounds, the significant range of solubility of the 2-2-1 ternary indides[13] provides the possibility to investigate the effect of electronic concentration. Particularly, within the region where In sites can be occupied by Pd atoms, the number of "holes" in the conduction band is expected to increase driven by Pd concentration. For such a purpose, we have performed a systematic study of the low-temperature magnetic properties of $Ce_{2-x}Pd_{2+y}In_{1-z}$ alloys within a broad range of composition.

II. EXPERIMENTAL DETAILS AND RESULTS

The metals used for sample preparation were palladium (foil, 99.95 mass % purity, Chimet, Arezzo, Italy), cerium (bar, 99.99 mass % purity, NewMet Kock, Waltham Abey, UK), and indium (ingot, 99.999 % mass purity, Johnson Matthey, London, UK). The samples, each with a total weight of about 2 g, were prepared by weighing the proper amounts of elements and then by argon arc melting the elements on a water-cooled copper hearth with a tungsten electrode. To ensure good homogeneity, the buttons were turned over and remelted several times. Weight losses after melting were always smaller than 0.5 mass %. All the samples were then annealed at 750 °C for 10 days, and finally quenched in cold water. A scanning electron microscopy (SEM) supplied by Carl Zeiss SMT Ltd. Cambridge, England, and electron probe microanalysis (EPMA) based on energy-dispersive x-ray spectroscopy were used to examine phase compositions. Smooth surfaces of specimens for microscopic observation were prepared by using SiC papers and diamond pastes down to 1 μm grain size. The compositional contrast was revealed in unetched samples by means of a backscattered electron detector (BSE). For the quantitative analysis, an acceleration voltage of 20 KV was applied for 50 s, and a cobalt standard was used for calibration. The composition values derived were usually accurate to 1 at.%. X-ray diffraction (XRD) was performed on powder samples using the vertical diffractometer X-Pert MPD (Philips, Almelo, The Netherlands) with Cu $K\alpha$ radiation.

Specific heat was measured using a standard heat pulse technique in a semiadiabatic He-3 calorimeter in the range between 0.5 and 20 K, at zero and applied magnetic field up to 2 T. Dc-magnetization measurements were carried out using a standard SQUID magnetometer operating between 2 and 300 K, and as a function of field up to 5 T. For ac-susceptibility measurements, a lock-in amplifier was used operating at 1.28 KHz, with an excitation field of 10^{-4} T on compensated secondary coils in the range of 0.5–10 K.

The Ce_2Pd_2In system presents a wide range of solid solution,[13] with a gap of solubility around the stoichiometric composition. Such a gap splits the range of solubility into two branches that show distinct magnetic structures, with the Ce-rich branch being FM and the Pd-rich one AF.[13] The alloys investigated in this work can be described by the general formula $Ce_{2-x}Pd_{2+y}In_{1-z}$, with $-0.1 \leqslant x \leqslant 0.1$, $y = x + z$, and $0.05 \leqslant z \leqslant 0.3$, with the richest Pd composition placed at the edge of the chemical stability. Most of the work was performed on the AF branch by substituting some In atoms for Pd ones. However, one alloy from the FM branch (cf. $Ce_{2.1}Pd_{1.95}In_{0.95}$) was also investigated for comparison with the aim of extending the study of the electron concentration effect over the solubility gap.

Concerning the structural consequences of the Pd/In substitution in the alloys belonging to the Pd-rich AF branch, one can recognize from the compositional dependence of the lattice parameters that the volume cell is practically unchanged. There is, however, a slight decrease of the a lattice parameter accompanied by an increase of the c parameter, which produces an increase of the c/a ratio. Such a variation is explained by the fact that the excess of Pd replacing larger In atoms occupies two 4e sites that lie on the c axis symmetrically placed with respect to the original In-2a site.[13] As a consequence, the Ce-Ce interplane distance is expected to increase with Pd content.

A. Thermal properties

In Fig. 1, we compare the thermal dependence of the magnetic contribution to the specific heat for samples with concentration $Pd_{2+y} = 2.20$, 2.25, 2.35, and 2.40, all of them belonging to the Pd-rich AF branch. The magnetic contribution $C_m(T)$ is computed by subtracting the $C_P(T)$ results from

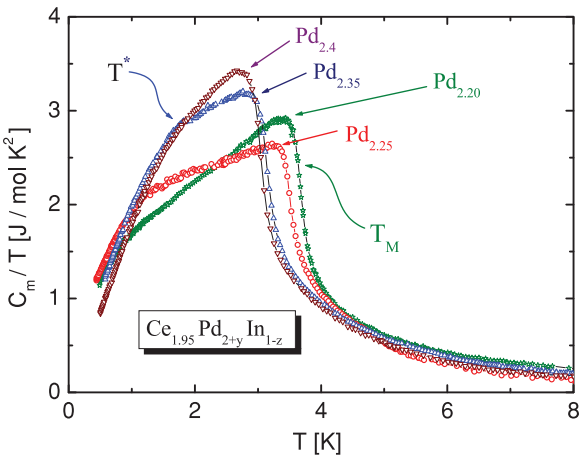

FIG. 1. (Color online) Thermal dependence of the magnetic contribution to specific heat C_m divided by T for different Pd concentrations, showing two characteristic temperatures: the AF transition T_M associated with the maximum of C_m/T and a shoulder labeled T^*.

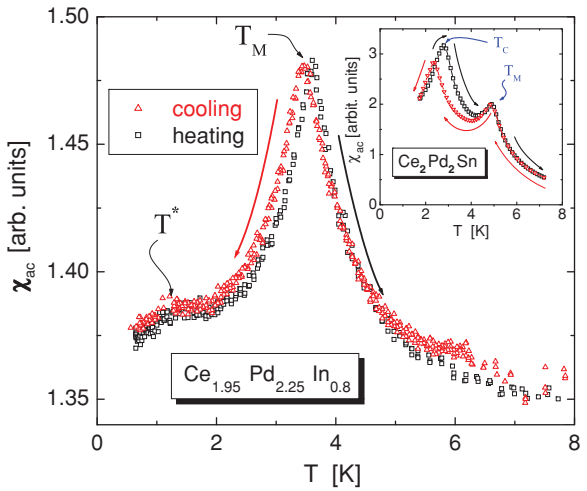

FIG. 2. (Color online) Low-temperature ac susceptibility of $Ce_{1.95}Pd_{2.25}In_{0.8}$. Inset: comparison with Ce_2Pd_2Sn after Ref. 10.

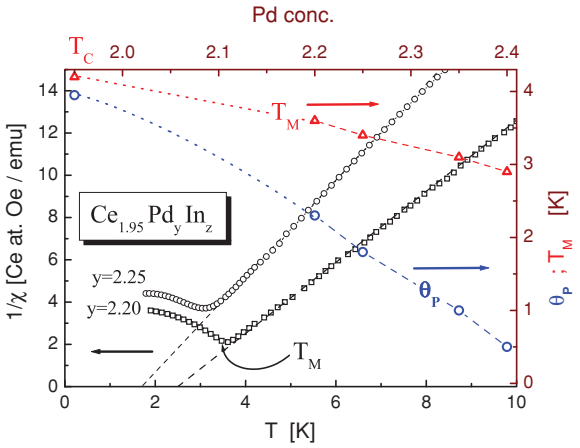

FIG. 3. (Color online) Low-temperature inverse susceptibility (B/M, with $B = 0.3$ T) of two samples showing the paramagnetic temperature extrapolation θ_P on the left and lower axes. The Pd concentration dependence of θ_P and the susceptibility cusp at $T = T_M$ correspond to the right and upper axes, including the T_C of one FM sample. The dotted lines indicate the respective extrapolations of θ_P and T_M from the AF samples (connected by dashed lines) to the values of the only FM sample on the left extreme of the figure.

the nonmagnetic isotypic La compound to the total measured values. In the figure, two characteristic temperatures can be seen: (i) one associated with a clear change in the C_m/T slope at a temperature labeled T^* that increases from ≈ 0.9 to 1.7 K between $Pd_{2+y} = 2.20$ and 2.35, but smearing out at 2.40, and (ii) the AF transition at $T = T_M$ (defined as the maximum slope of C_m/T), which decreases from 3.7 to 3.0 K. Notably, the maximum value of C_m/T_M first decreases between $Pd_{2+y} = 2.20$ and 2.25, and then increases up to $Pd_{2+y} = 2.40$. Such a nonmonotonous behavior can be attributed to competing factors that change differently with Pd concentration, for example, an increasing degree of disorder as the composition moves away from stoichiometry and the fact that the C_m/T_M ratio increases as T_M decreases.

Contrary to Ce_2Pd_2Sn, there is no first-order transition (like T_C), but a shoulder at the temperature $T = T^*$ where the modulated phase[13] transforms into the FM GS. To check this difference between indides and stannides, we have measured the ac susceptibility χ_{ac} on the $Pd_{2+y} = 2.25$ alloy, see Fig. 2. The $\chi_{ac}(T)$ maximum at $T = 3.6$ K coincides with the corresponding T_M value, but only a weak shoulder is detected at $T = 1.5$ K in coincidence with $C_m(T)/T$. This temperature dependence has to be compared with that of Ce_2Pd_2Sn (Ref. 10) shown in the inset. There, the first-order character of the lower transition is clearly evidenced by the thermal hysteresis around T_C. On the contrary, the low signal and the lack of thermal hysteresis at T^* in the indide compound indicates that no magnetic transition occurs at that temperature.

B. Magnetic properties

The T_M(Pd) dependence was also traced by $M(T)$ measurements. In Fig. 3, we show the inverse of the low-temperature susceptibility measured with $B = 0.3$ T on two representative samples: $Ce_{1.95}Pd_{2.2}In_{0.85}$ and $Ce_{1.95}Pd_{2.25}In_{0.8}$. The respective paramagnetic temperatures θ_P and AF transitions T_M are depicted in Fig. 3 as a function of Pd concentration (right and upper axes) for all studied alloys, including a FM one with $Pd_{2+y} = 1.95$. One can see that θ_P(Pd) rapidly decrease with Pd content, extrapolating to zero for $Pd_{2+y} \approx 2.43$, whereas T_M(Pd) decreases moderately.

The measurement performed up to room temperature on the $Ce_{1.95}Pd_{2.20}In_{0.85}$ sample (not shown) allowed us to evaluate the magnetic moments of the ground and excited crystal field (CF) levels, and their respective CF splitting. For such a purpose, we have used the simplified formula[14]

$$M/B = \sum_0^2 \mu_i^2 \exp(-\Delta_i/T)/[(T - T_I)Z], \qquad (1)$$

where μ_i are the effective moments of the ground state ($i = 0$) and excited CF levels ($i = 1,2$, respectively) and T_I practically equals θ_P. The values obtained for the ground and first CF excited levels are $\mu_0 = 1.6\mu_B$ and $\mu_1 = 2.4 \pm 0.2\mu_B$, with a CF splitting $\Delta_1 = 60 \pm 5$ K. These values are very similar to those obtained for Ce_2Pd_2Sn (Ref. 10) and guarantee that only the GS doublet is responsible for the low-temperature properties. As a consequence of the good fit obtained by applying Eq. (1) without including any $4f$ conduction-band hybridization effect, it can be concluded that this system can be considered as formed by a Ce^{3+} ion lattice with an irrelevant Kondo effect (i.e., $T_K < T_M$, where T_K is the Kondo temperature).

C. Field dependencies

The temperature dependence of magnetization $M(T)$ was studied in all the samples under different applied fields up to $B = 0.7$ T to obtain the respective magnetic phase diagrams. In Fig. 4, we present a detailed investigation performed on the $Ce_{1.95}Pd_{2.20}In_{0.85}$ alloy, selected for having its composition closer to stoichiometry. Even though these $M(T)$ curves of equal field intensity (cf. isopedias) were measured between $1.8 \leqslant T \leqslant 20$ K, they are only shown up to 10 K for clarity. The $M(B)$ isotherm obtained at our lowest measured

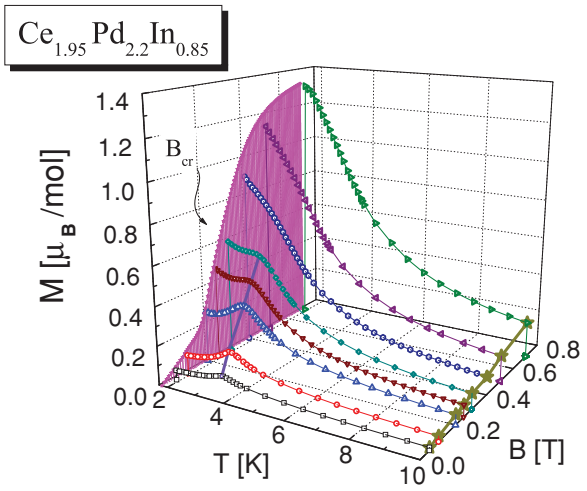

FIG. 4. (Color online) Thermal dependence of the magnetization for different applied fields. At $T = 1.8$ K, an $M(B)$ is included and the continuous line at $T \approx 3$ K connects the $M(T_M)$ cusps. B_{cr} indicates the critical field at which the $T_M(B)$ transition vanishes. A continuous line shows the $M(B)$ dependence at $T = 10$ K.

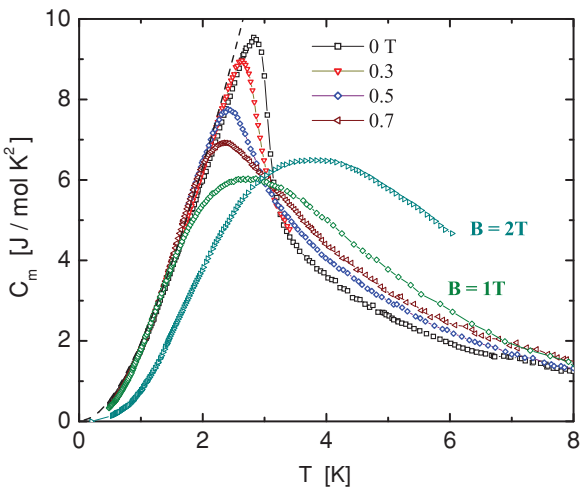

FIG. 5. (Color online) Magnetic-field effect on the specific heat of $Ce_{1.9}Pd_{2.4}In_{0.7}$ up to $B = 2$ T. The dashed curve is the fit for $B = 0$ T using Eq. (2).

temperature ($T = 1.8$ K) is also included in the M-B plane. These $M(T)$ curves show an AF-type behavior up to about $B = 0.18$ T, turning into a field-induced FM polarization at higher field. As this polarization arises, it overcomes the T_M transition defined as the cusp of $M(T)$ (see the continuous curve around $T = 3$ K in Fig. 4). This indicates that the ShaSu phase is suppressed at a critical field B_{cr} slightly above $B = 0.3$ T. Notably, T_M itself is slightly affected by magnetic field because in that alloy it decreases from 3.56 K at 50 mT to 3 K at 0.3 T. This means that the intensity of the J and J' couplings is weakly affected by field despite the degrees of freedom progressively transferred to the FM phase. This field dependence for all the studied alloys is included in the magnetic phase diagrams presented at the end of Sec. III.

The magnetic-field effect on the specific heat $C_m(T)$ was also studied in all the samples, however more detailed measurements were carried out on the richest Pd sample $Ce_{1.9}Pd_{2.4}In_{0.7}$, up to $B = 2$ T, as shown in Fig. 5. Since this alloy lies at the edge of the solid solution formation, we have chosen it for the field-effect investigation to drive T_M to lower temperature and to trace the disappearance of the T^* shoulder. The temperature of the $C_M(T)$ maximum [coincident with T_M defined by the cusp in $M(T)$] progressively decreases with field until it reaches the value of T^* at $B_{cr} = 0.7$ T. Beyond that value, the $C_m(T)$ maximum broadens and starts to increase in temperature with a typical behavior of a FM field-polarized system. Coincidentally, the $C_m(T_M)$ jump is overcome by the high-temperature tail of $C_m(T > T_M)$, indicating an increase of the magnetic correlations prior to the transition. Up to $B = 0.5$ T, the low-temperature ($T < T^*$) $C_m(T)$ dependence practically coincides, without affecting substantially the gap of anisotropy or the $T^{1.5}$ coefficient determined applying Eq. (2); see the next section. Since $C_m(T)$ curves cross each other (at ≈ 3 K), one may conclude that there are degrees of freedom transferred from the intermediate phase (i.e., $T^* < T < T_M$) to the region where dimers form (i.e., $T > T_M$). On the contrary, no degrees of freedom are transferred from $T < T^*$ by the magnetic-field effect. This indicates that the FM GS is more robust under field than the intermediate phase between T_M and T^*.

III. DISCUSSION

The magnetic nature of the GS can be recognized by analyzing the thermal dependence of the specific heat. Below T^*, the $C_m(T)$ dependence is properly fitted according to an anisotropic FM relation dispersion like that observed in Ce_2Pd_2Sn:[10]

$$C_m(T < T^*) = \gamma T + AT^{3/2} \exp(-\Delta_M/T), \qquad (2)$$

where γ is the Sommerfeld coefficient and Δ_M a gap in the magnon spectrum, which rises from zero for $Pd_{2+y} = 2.2$ up to 0.4 K for the $Pd_{2+y} = 2.4$. Such an increase of Δ_M indicates an increasing anisotropy driven by the fact that the Ce-Ce inter-plane distance expands from 3.963 to 4.017 Å.[13] The γ coefficient extracted for these Pd-rich AF alloys is comparable to that of the La isotypic compound, in agreement with the expected Ce^{3+} character of the magnetic ions and the consequent negligible Kondo effect.

For the case of the studied Ce-rich FM alloy $Ce_{2.1}Pd_{1.95}In_{0.95}$, a similar thermal dependence is observed, with $C_m = 0.14 + 4.3T^{3/2} \exp(-2.8/T)$ up to T_C; see Fig. 6. A FM-type dispersion relation is certainly expected from the spontaneous magnetization observed in $M(T)$ below $T_C = 4$ K. However, the large $\gamma = 0.14$ J/mol K^2 is somehow unexpected from the 3^+ character of the Ce atoms and in comparison with that of the AF alloys. This enhanced contribution can be explained by a closer inspection to the interatomic Ce-Ce spacing on the Ce-rich FM branch provided in Ref. 13. Although Ce-Ce spacing on the plane increases slightly following the a lattice parameter, the situation around the extra Ce atom loci on the $z = 0$ plane (at the $2a$ Wyckoff position) is quite different. Due to the larger atomic radius of Ce atoms with respect to In ones, the substituted atoms support a significant "crystal pressure," which reduces the Ce-Ce spacing below the magnetic limit. As a consequence,

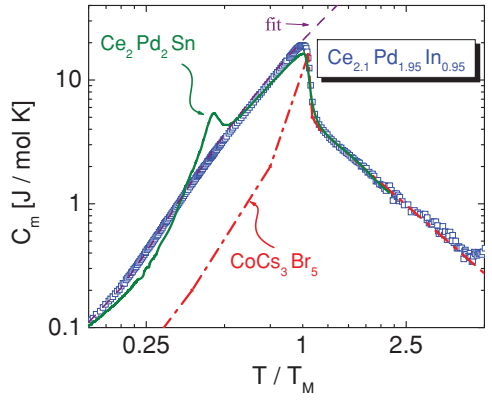

FIG. 6. (Color online) Comparison of the specific-heat magnetic contribution of two Ce_2Pd_2X (X = In and Sn) compounds with the model compound for a 2D simple square lattice $CoCs_3Br_5$ (dashed-dotted line). The temperature axis is normalized to the respective ordering temperatures. The dashed curve is the fit to $Ce_{2.1}Pd_{1.95}In_{0.95}$ using Eq. (2).

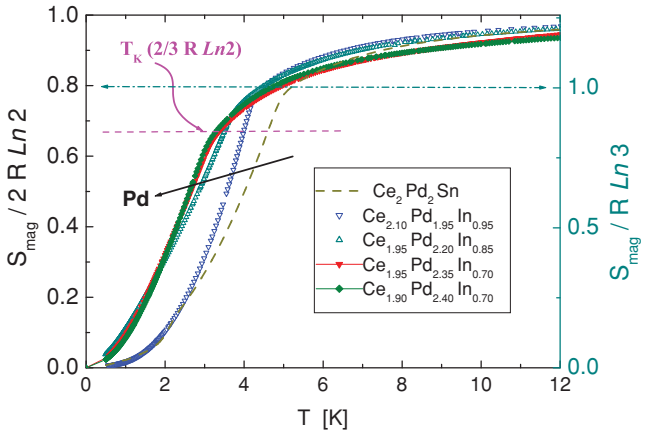

FIG. 7. (Color online) Comparison of the thermal increase of the entropy between indide and stannide compounds, including Ce_2Pd_2Sn (Ref. 10) as reference. The entropy contribution is re-normalized with respect to two Ce atoms per formula unit. Notice that the thermal evolution and the entropy of $Pd_{2.35}$ and $Pd_{2.40}$ practically overlap all along the temperature range. The dashed-dotted line compares the entropy between two single atoms with effective spin $S_{\rm eff} = 1/2$ and one FM dimer with $S_{\rm eff} = 1$ (see the text). The dashed line indicates the isentropic value $T_K \simeq 2/3R\ln 2$ from which the Kondo temperature is evaluated (see the text). The arrow indicates the direction of Pd concentration increase.

hybridization effects may arise between those substituent atoms and their Ce-NN on the $4h$ position in the $z = 0$ plane. In such a case, those atoms may contribute to the specific heat as Kondo impurities, increasing the γ coefficient.

Concerning the low-temperature properties presented in Fig. 3, there is an apparent contradiction between the positive value of θ_P expected for a FM system and the AF-like cusp in the temperature dependence of the susceptibility. As in Ce_2Pd_2Sn, this fact indicates that two contributions are competing at that temperature. Both mechanisms are intrinsic to the formation of a ShaSu lattice because the FM J coupling is responsible for the dimer formation above T_M and the AF J' couples those dimers to build up the ShaSu network below T_M.

A. Dimer formation

Since the objective of this work is to investigate the effect of electronic (holes) variation on the ShaSu lattice stability, the first issue is to ascertain whether dimers actually form in these alloys as they do in Ce_2Pd_2Sn.[10] The second is to check whether the magnetic phase below T_M maintains the characteristics assigned to ShaSu lattices once Sn[$5s^25p^2$] is replaced by In[$5s^25p^1$] and the number of holes is increased further by Pd concentration.

Following the same procedure proposed in Ref. 10, we have evaluated the magnetic entropy gain $S_{\rm mag}(T)$ from the measured specific heat as $S_{\rm mag} = \int C_m/T\,dT$, and included those results in Fig. 7 for different Pd concentrations, including one Ce-rich FM alloy $Ce_{2.1}Pd_{1.95}In_{0.95}$. For the latter compound, it can be seen that the "per Ce atom" entropy at $T = T_M$ is $S_{\rm mag} = 0.8R\ln 2$, which coincides with the molar entropy of $R\ln 3$. As was analyzed in Ref. 10, this entropy value corresponds to a FM-dimer formation since its effective spin $S_{\rm eff} = 1$ is threefold degenerate (in contrast to the $S_{\rm eff} = 1/2$ doublet of a single moment). Just as for the stoichiometric compound Ce_2Pd_2Sn,[10] which is included in the figure as a reference, the formation of FM dimers is inferred for the FM indide. The remaining entropy is collected above the transition since the onset of magnetic correlations occurs at $T \leqslant 20$ K as indicated by the $C_m(T > T_M)$ tail in Fig. 6. Notice that for the $Ce_{2.1}Pd_{1.95}In_{0.95}$ compound, $C_m(T > T_M)$ coincides nicely with that of the model compound for the 2D-square lattice $CoCs_2Br_5$ (Ref. 15) and the parent compound Ce_2Pd_2Sn.

For the alloys belonging to the AF branch, the entropy at T_M decreases progressively and the criterion to compare $S_{\rm mag} = 0.8R\ln 2$ with $R\ln 3$ only applies to the sample close to the stoichiometry, that is, $Pd_{2+y} = 2.2$. For higher Pd concentrations, the entropy evaluation has to be normalized to the actual number of Ce atoms not affected by the proximity of a double Pd occupation in sites $4e$. This renormalization may include the $Pd_{2+y} = 2.25$ sample into those where Ce-Ce dimers are formed, but it does not apply satisfactorily to the samples with $Pd_{2+y} = 2.35$ and 2.4. Nevertheless, the increase of doubly occupied $4e$ sites progressively destroys the lattice character of the ShaSu network.

The value of the Kondo temperature for this system can also be determined from the $S_{\rm mag}(T)$ results shown in Fig. 7 by applying the Desgranges-Schotte[16] criterion of $S_{\rm mag}(T = T_K) \simeq 2/3R\ln 2$ for a nonordered system. As shown in Fig. 7, $T_K \approx 3$ K, which is similar to the value found for the parent compound Ce_2Pd_2Sn.[10] This is one of the lowest values found among the Ce compounds and confirms the Ce^{3+} character of this ion.

B. Shastry-Sutherland lattice symptoms

As mentioned in the Introduction, one of the characteristic features observed in the exemplary compounds exhibiting a ShaSu lattice is the crossing of the $M(B)$ isotherms at low temperatures. To search for this effect in the family of compounds under study, we have chosen the $Ce_{1.95}Pd_{2.2}In_{0.85}$ alloy because

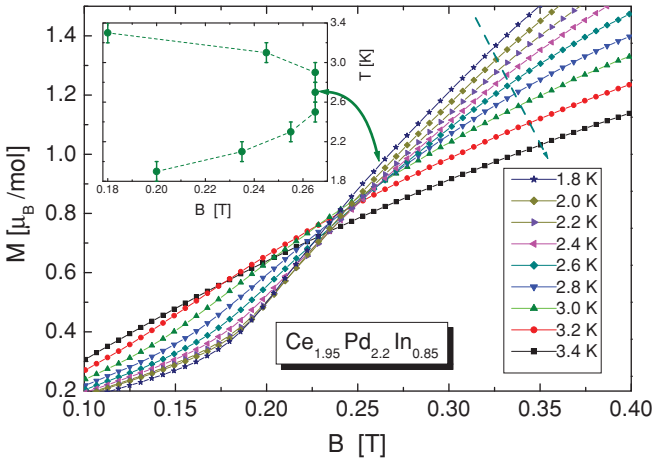

FIG. 8. (Color online) Detail of the M vs B isotherms of the $Ce_{1.95}Pd_{2.2}In_{0.85}$ sample in the region where the crossing occurs. In the inset, the temperature and field values of the crossing points are depicted. Since the crossing corresponds to two neighboring isotherms, the points are depicted as a function of their respective mean temperature values.

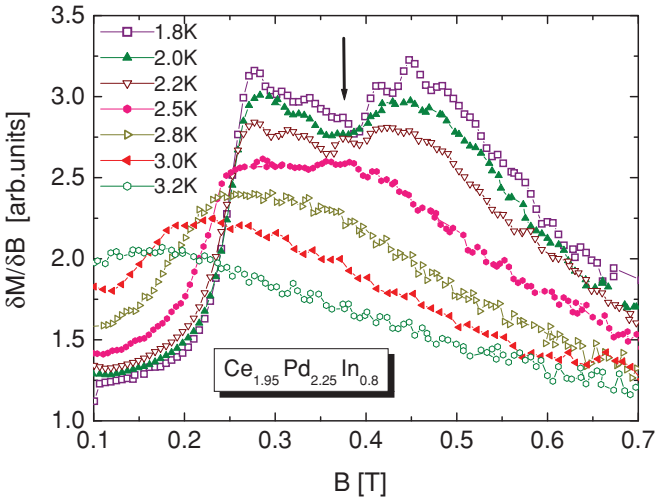

FIG. 9. (Color online) Field dependence of the $M(B)$ derivative to show a relative minimum related to an incipient step in M vs B isotherms, indicated by the arrow.

it shows the more pronounced change of slope of $M(B)$ within our range of measurement. In Fig. 8, we show the detailed study of those isotherms in the region of temperature between $1.8 \leqslant T \leqslant 3.4$ K. Within the experimental dispersion, it can be seen that such a crossing occurs between $2.4 \leqslant T \leqslant 3$ K at a field $B = 0.26 \pm 0.05$ T, where the magnetic moment is $M = 0.89 \pm 0.01 \mu_B$/mol; see the inset in Fig. 8. For higher Pd concentration (cf. $Pd_{2+y} = 2.25$), the crossing occurs at higher field and slightly lower temperature, albeit the slope of the isotherms is not so pronounced and the effect practically vanishes for $Pd_{2+y} = 2.35$.

Some thermodynamic consequences can be deduced from the existence of such a crossing. Since within that range of temperature the magnetization does not change, then $\partial M/\partial T\,|_B = 0$, and from Maxwell relations also $\partial S/\partial B\,|_T = 0$ is deduced. This implies the existence of an "isosbestic" point,[17] which should be reflected in the corresponding thermodynamic parameters like $C_m(T,B)/T$. Effectively, specific heats measured at $B = 0$ and 0.5 T (not shown) cross each other at about 2.9 K.

The other characteristic of the ShaSu is the appearance of quantized $M(B)$ steps. From the measurements of the $M(B)$ isotherms, this feature was not observed, probably due to the polycrystalline nature of the samples. However, the analysis of their derivatives, $\partial M/\partial B\,|_T$, allows us to detect an incipient structure as a function of field, as is shown in Fig. 9. Notice that for that figure, we have selected the $Ce_{1.95}Pd_{2.25}In_{0.8}$ alloy because the discussed effect occurs at higher temperature by increasing Pd content. Such a procedure allows us to observe the split maximum within a larger range of temperature. Further increase of Pd, that is, for $Pd_{2+y} = 2.35$ and 2.4, strongly weakens the $M(B)$ curvature smearing out the effect. As shown in Fig. 9, the minimum related to the incipient step occurs at $B \approx 0.4$ T, where $M(B) = 0.4\mu_B$ is $\approx 1/4 M_{sat}$ since M_{sat} is about $1.3\mu_B$.[13]

Note the comparison between the different fields at which the $M(B)$ steps occur and the nearly constant temperature of the crossing of M isotherms for the different mentioned systems. While in $Sr_2Cu(BO_3)_2$ the plateaus occur at very high field $B \approx 20$ T, in metallic RB_4 it occurs around $4 < B < 8$ T depending on the crystallographic directions, and at much lower B (a fraction of Tesla) in R_2T_2X compounds. In spite of that, the crossing of $M(B)$ isotherms always occurs at low temperature ($T < 4$ K). This significant difference between magnetic and thermal scales supports the role of the "quantized magnetization" constrain, making relevant the fact that these effects are related to fractional M/M_{sat} values. Since in $SrCu_2(BO_3)_2$ a superexchange mechanism drives the magnetic interactions, high applied field is required to reverse the magnetic nature of the GS in the singlet-triplet level spectrum of the dimers. On the contrary, for Ruderman-Kittel-Kasuya-Yosida (RKKY) -mediated magnetic interactions, such a singlet-triplet modification is expected to be much weaker, and consequently a lower field would induce the "quantized

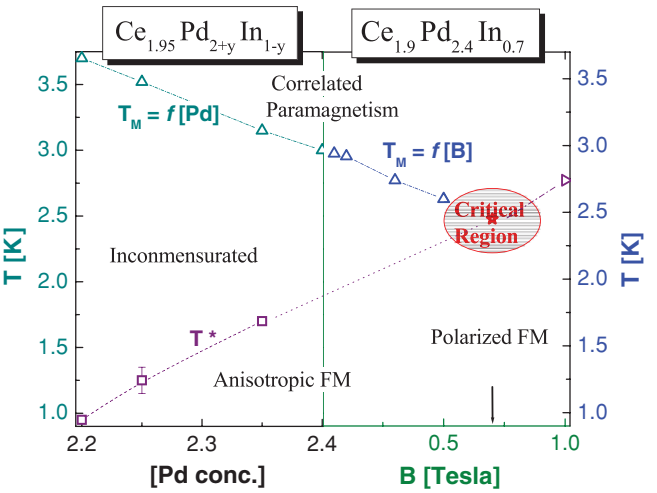

FIG. 10. (Color online) Magnetic phase diagram as a function of (a) Pd concentration and (b) field dependence for the $Pd_{2.4}$ sample. The arrow indicates the critical field at which the minimum value of $T_{max}(C_P)$ is observed.

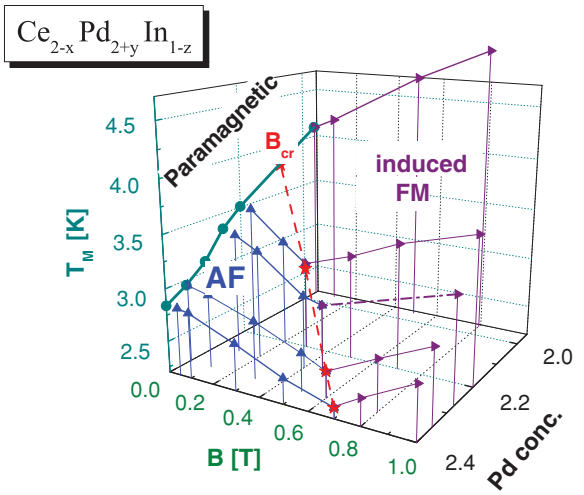

FIG. 11. (Color online) 3D representation of the magnetic phase diagram as a function of Pd concentration and magnetic field. Dashed (red) line connects the critical fields B_{cr}(Pd) of each Pd concentration.

magnetization jumps." On the other hand, the crossing effect depends on the relative thermal population of the levels. Once the field-driven values for the appropriated M/M_{sat} values are reached, field-independent thermal excitations produce the "crossing effect." In other words, this $M(T)$ effect cannot be scaled as $M(B/T)$.

C. Magnetic phase diagram

The magnetic phase diagram as a function of Pd concentration is shown in Fig. 10(a) (left side) with T_M defined as the temperature of the maximum value of $C_m(T)$ and T^* as the temperature of the maximum curvature of $C_m(T)/T$ defined as a kink for $Pd_{2+y} = 2.20$ and 2.25, and as a "shoulder" for $Pd_{2+y} = 2.35$ and 2.40 in Fig. 1.

This y(Pd)-dependent phase diagram is complemented by the field dependence of the $Pd_{2+y} = 2.4$ sample after an appropriated scaling between Pd concentration and magnetic field on the right side of Fig. 10(b). Since this sample is at the edge of the solid solution, the magnetic-field application allows us to access a critical point that cannot be reached by increasing Pd content. With such a scaling between Pd concentration and magnetic field, a $Pd_{2+y} = 2.54$ value is extrapolated. Although the second-order character of the magnetic transition smears progressively out in the $Pd_{2+y} = 2.4$ sample under applied field, the maximum of $C_m(T,B)$ allows us to extend the upper phase boundary up to a magnetic critical point at $T_{cr} = 2.3$ K and $B_{cr} = 0.7$ T.

A 3D representation of the magnetic phase diagram is presented in Fig. 11 as a function of both control parameters—magnetic field and Pd concentration—to compare the B dependence of all the AF alloys. In this diagram, one of the Ce-rich FM samples (cf. $Pd_{2+y} = 1.95$) is also included for the purpose of testing the Pd concentration (i.e., the "hole" concentration) as a unique parameter able to encompass the alloys studied in this work, even beyond the gap of miscibility. No further extrapolation on the Pd dependence can be done within the Ce-rich FM side because in that "branch" of the phase diagram, the free concentration parameter is the Ce composition while the Pd remains constant.[13]

The minima of T_M as a function of field observed in the AF alloys indicate that the critical field B_{cr}, where the polarized FM behavior takes over, increases with Pd content. As expected, the magnetic boundary for $Pd_{2+y} = 2.4$ coincides with the right side of Fig. 10. Notably, the extrapolation of $B_{cr}(y) \to 0$ occurs at $Pd_{2+y} = 2.1$, which lies within the gap between AF and FM branches but leaves a unique FM folder on the right side.

IV. CONCLUSIONS

The magnetic properties of the $Ce_{2-x}Pd_{2+y}In_{1-z}$ family of compounds can be described as a function of a unique parameter: the decrease of the electronic concentration, and consequently their Fermi energy, as the number of "holes" increases with Pd concentration.

Their ground state shows a common ferromagnetic character in their magnon dispersion extracted from the specific heat at low temperature. This is confirmed by magnetization measurements. However, the transition from their respective paramagnetic states is different depending on the relative Ce/Pd concentration. The rich Ce sample shows a typical FM transition. On the contrary, the rich Pd ones show a transition with AF characteristics that become FM after a characteristic temperature T^*.

Since the value extracted for the Kondo temperature is extremely low, the magnetic $4f$ states of the Ce ions are strongly localized all along the series. Nevertheless, in the Ce-rich sample, the Ce atoms substituting In seem to behave differently since their available volume is considerably smaller.

The conditions for dimers formation are realized only in the alloys lying closer to stoichiometry, that is, in the $Pd_{2+y} = 2.20$ and 2.25 ones. Higher Pd concentration distorts the Ce lattice, inhibiting the formation of a well-defined network of those dimers. This reveals the instability of the ShaSu lattice due to atomic disorder.

Concerning the ShaSu phase symptoms in the $Pd_{2+y} = 2.20$ and 2.25 alloys, the $M(B)$ isotherm crossing is observed in the alloys of that AF branch. However, only an incipient modulation in the $M(B)$ dependence is seen in its derivative. The polycrystalline character of this system may explain the weakness of this effect together with its intermetallic nature since the electrons in the conduction band (responsible for the RKKY interaction) are strongly delocalized.

An interesting complement to this research might be to drive the weakening of the Ce^{3+} moments by chemical pressure.

ACKNOWLEDGMENTS

We acknowledge J. Luzuriaga for his help with the magnetic measurements, P. Pedrazzini for carefully reading the manuscript, and P. Carretta for fruitful discussions. This work was partially supported by a CNR (Italy) and CONICET (Argentina) cooperation program, PICTP-2007-0812 and Secyt-UNC 06/C256 projects.

[1]See, e.g., C. Lacroix, J. Phys. Soc. Jpn. **79**, 011008 (2010).
[2]B. S. Shastry and B. Sutherland, Physica **108B**, 1069 (1981).
[3]H. Kageyama, K. Yoshimura, R. Stern, N. V. Mushnikov, K. Onizuka, M. Kato, K. Kosuge, C. P. Slichter, T. Goto, and Y. Ueda, Phys. Rev. Lett. **82**, 3168 (1999).
[4]S. Miyahara and K. Ueda, Phys. Rev. Lett. **82**, 3701 (1999).
[5]S. Michimura, A Shigekawa, F. Iga, M. Sera, T. Takabatake, K. Ohoyama, and Y. Okabe, Physica B **378-380**, 596 (2006).
[6]M. S. Kim, M. C. Bennett, and M. C. Aronson, Phys. Rev. B **77**, 144425 (2008).
[7]F. Fourgeot, P. Gravereau, B. Chevalier, T. Roisnel, and J. Etorneau, J. Alloys Compd. **238**, 102 (1996).
[8]M. Giovannini, H. Michor, E. Bauer, G. Hilscher, P. Rogl, and R. Ferro, J. Alloys Compd. **280**, 26 (1998).
[9]M. N. Peron, Y. Kergadallan, J. Rebizant, D. Meyer, S. Zwirner, L. Havela, H. Nakotte, J. C. Sprilet, G. M. Kalvius, E. Colineau, J. L. Oddou, C. Jeandey, and J. P. Sanchez, J. Alloys Compd. **201**, 203 (1993).
[10]J. G. Sereni, M. Gomez-Berisso, A. Braghta, G. Schmerber, and J. P. Kappler, Phys. Rev. B **80**, 024428 (2009).
[11]J. G. Sereni, M. Gomez-Berisso, G. Schmerber, and J. P. Kappler, Phys. Rev. B **81**, 184429 (2010).
[12]J. G. Sereni, J. Phys. Conf. Ser. (to be published).
[13]M. Giovannini, H. Michor, E. Bauer, G. Hilscher, P. Rogl, T. Bonelli, F. Fauth, P. Fischer, T. Herrmannsdorfer, L. Keller, W. Sikora, A. Saccone, and R. Ferro, Phys. Rev. B **61**, 4044 (2000).
[14]J. G. Sereni, T. Westerkamp, R. Kuchler, N. Caroca-Canales, P. Gegenwart, and C. Geibel, Phys. Rev. B **75**, 024432 (2007).
[15]R. F. Wielinga, H. W. Blöte, J. A. Roest, and W. J. Huiskamp, Physica **34**, 223 (1967).
[16]H.-U. Desgranges and K. D. Schotte, Phys. Lett. A **91**, 240 (1982).
[17]M. Eckstein, M. Kollar, and D. Vollhardt, J. Low Temp. Phys. **147**, 279 (2007).